# SAMS: A SENSITIVITY ANALYSIS MODULE FOR CRITICALITY SAFETY ANALYSIS USING MONTE CARLO TECHNIQUES

Bradley T. Rearden
Oak Ridge National Laboratory
P.O. Box 2008
Oak Ridge, TN 37831-6730
reardenb@ornl.gov

## ABSTRACT

The SAMS module has been developed to calculate the relative change in the value of $k_{eff}$ due to a change in a constituent component or cross section. The SAMS module works in conjunction with a modified version of the CSAS25 sequence of SCALE that employs an enhanced version of KENO V.a, which is capable of calculating the spherical harmonics components of the flux moments. The SAMS module performs sensitivity calculations using linear perturbation theory as implemented in the FORSS system and requires the calculation of the forward and adjoint flux moments with the enhanced version of KENO V.a.

SAMS automatically selects all of the sensitivity parameters that can be calculated for each nuclide in each region of the system based on available cross-section data. Sensitivity parameters for a given nuclide may be generated for a number of parameters, including total, scatter, capture, and fission cross sections, as well as $\bar{n}$ and $\chi$. The sensitivities for any nuclide-reaction pair calculated with SAMS can be output on three bases: group-wise region dependent, energy-integrated region dependent, and energy- and region-integrated.

The sensitivities generated with SAMS have been verified through comparisons with those generated with the SEN1 and SEN2 sensitivity sequences of SCALE. SAMS is capable of producing accurate sensitivities, provided the KENO V.a regions have been appropriately subdivided to allow for sufficient resolution of the flux moments throughout the problem geometry.

# 1. INTRODUCTION

Extensive work has recently been conducted to demonstrate that sensitivity and uncertainty analysis methodologies can be used to help establish areas of applicability and the related validation of computational codes and data for nuclear criticality safety.[1] In this work, three methodologies have been demonstrated to quantitatively establish areas of applicability and to establish code and data biases. These procedures are based on sensitivity and uncertainty (S/U) analysis methodologies and include integral parameter applications, uncertainty analysis theory and generalized-linear-least-squares methodology (GLLSM). In each of the three methodologies, group-wise sensitivity profiles for multiple nuclides and reactions are required to perform the analyses. These sensitivities predict the relative change in the system $k_{eff}$ due to a perturbation in a constituent cross-section data component.

For compatibility with other analysis techniques at ORNL, it is desirable to generate these sensitivity profiles through the implementation of perturbation theory codes (PTC) in the SCALE (Standardized Computer Analyses for Licensing and Evaluation) code system.[2] The methodology of choice for calculating sensitivity and uncertainty parameters in SCALE was first used in the Fantastic Oak Ridge Sensitivity System (FORSS).[3–5] The FORSS system was based on the widely used differential perturbation theory approach[6–9] and was capable of calculating the sensitivity of the system $k_{eff}$ to changes in group-wise cross-section data for any given isotope for a number of reaction types. The FORSS methodology requires the calculation of the forward and adjoint angular and scalar fluxes and flux moments. Once these flux solutions are determined, the relative change in the system $k_{eff}$ due to a change in a component cross section can be determined. These sensitivities are calculated for each material region, nuclide, reaction type and energy group in the system model.

Recently, the FORSS methodology was updated and applied to the SCALE code system for one-, two- and three-dimensional criticality safety analyses. The SEN1 and SEN2 sequences use deterministic neutron transport to calculate the necessary forward and adjoint neutron fluxes in 1- and 2-D, respectively.[10] The prototypic **S**ensitivity **A**nalysis **M**odule for **S**CALE (SAMS),[11] presented in this paper, utilizes 3-D Monte Carlo techniques to generate the necessary fluxes and computes sensitivity parameters and their associated uncertainties, utilizing the FORSS techniques. It was designed to work in conjunction with the CSAS25 analytical sequence. This sequence is commonly used to analyze criticality safety problems, and many institutions already possess input decks for the CSAS25 sequence that could be modified for sensitivity analysis with SAMS. Sensitivity profiles generated with SAMS can be used with S/U techniques to determine the range of applicability of a given set of critical experiment benchmarks.

# 2. METHODS

The application of the FORSS methodology to Monte Carlo techniques is presented in this section. The most complex component of this implementation is the calculation of the group to group transfer terms. Because the transfer (or scattering) cross sections are stored in a Legendre expansion, the neutron fluxes must be calculated in terms of the flux moments. In three

dimensions, this calculation requires a spherical harmonics expansion of the neutron flux. The "classical" approach to this solution is not well suited for application in Monte Carlo techniques. A new approach using angular transformations was developed to calculate the spherical harmonics components of the flux solution using Monte Carlo methods. The use of these flux moments in the FORSS methodology is also presented in this section.

## 2.1. CALCULATION OF FLUX MOMENTS

Deterministic neutron transport codes calculate the moments of the forward and adjoint fluxes for each region on a calculational mesh through a series expansion using spherical harmonics. Theoretically, this methodology could be applied to angular fluxes calculated through Monte Carlo methods. Based on an angular flux solution obtained over a discrete angular quadrature, the $j^{th}$ flux moments can be calculated as follows.[12]

$$\tilde{f}_{g,z}^{j} = \sum_{n=1}^{N} w_n R_n^j f_{g,z}^n \quad , \tag{1}$$

where

$f_{g,z}^n$ = neutron flux in region $z$, for direction $n$ and energy group $g$;
$w_n$ = weight function for direction $n$;
$R_n^j$ = real valued spherical harmonic function for moment index $j$ and quadrature direction $n$;
N = number of directions in the angular quadrature set.

Using the track length estimator method in a Monte Carlo calculation, the group-wise scalar flux within a single region for a single generation of particles is calculated as[13,14]

$$f_{g,z} = \frac{\sum_{k=1}^{K} wt_{k,z} l_{k,z}}{V_z \sum_{k=1}^{K} wt_{k,0}} \quad , \tag{2}$$

where

$l_{k,z}$ = distance traversed by particle k while within region z and energy group g;
$wt_{k,z}$ = weight of particle $k$ while traversing region $z$;
$V_z$ = volume of region $z$;
$wt_{k,0}$ = initial weight of particle $k$;
$K$ = total number of histories in the generation.

This method is easily modified to calculate the group-wise angular flux in a region as

$$f_{g,k}^{n} = \frac{\sum_{k=1}^{K} wt_{k,z} l_{k,z,n}}{V_z \sum_{k=1}^{K} wt_{k,0}} \quad , \tag{3}$$

where

$K$ = number of flux tallies in region $z$ for the current generation;

$l_{k,z,n}$ = the distance traversed by particle $k$ while within region $z$ and energy group $g$ within the solid angle $d\hat{\Omega}_n$ about the quadrature direction $\hat{\Omega}_n$.

However, it is not possible to obtain an accurate measure of the flux moments necessary for this implementation of sensitivity analyses with Monte Carlo methods. This is due to the geometry-modeling techniques typically used by Monte Carlo codes. For example, a system consisting of a homogeneous unreflected fueled sphere would typically be modeled in a Monte Carlo code as a single spherical region. Because the model of this system consists of only a single region, there would be only one value of the angular flux in each direction. Because this flux is isotropic, the angular flux solution for this problem is identical in all directions. If a symmetric level quadrature set is used, for a single group, all of the quadrature weights and angular fluxes are equal. Equation (3) can then be expressed as

$$\tilde{f}_{g,z}^{j} = \frac{f_{g,z}}{N} \sum_{n=1}^{N} R_n^j \, . \tag{4}$$

The summation in Eq. (4) is equal to zero when $j$ is equal to or greater than 1. The result is that moments of order 1 and higher for a single calculational zone are all exactly zero for a problem whose solution is isotropic on a system-wide scale. Deterministic codes calculate non-zero moments for the same problem for each interval in a fine calculational mesh. These moments add a significant contribution to the scattering sensitivities defined earlier. In typical Monte Carlo calculations, the flux moments are not necessary because scattering is treated as a probability and not as a reaction rate.

New techniques have been developed in this project to calculate flux moments via Monte Carlo methods. The higher-order flux moments are tallied in a method similar to that used to calculate the scalar flux. Each flux moment is calculated as

$$\tilde{f}_{g,z}^{j} = \frac{\sum_{k=1}^{K} R_k^j wt_{k,z} l_{k,z}}{V_z \sum_{k=1}^{K} wt_{k,0}} \, . \tag{5}$$

In Eq. (5) the spherical harmonics functions are calculated for each history using a transformed coordinate system such that the moments are based on a polar, rather than Cartesian, position

vector. This is a 3-D extension of the 1-D method for calculating the flux moments in terms of Legendre polynomials based only on $m$, the direction cosine with respect to the spatial coordinate. Through this technique, each tally is treated in a similar manner to each solution direction in discrete-ordinates techniques.

The spherical harmonics functions are calculated in a transformed coordinate system such that the transformed polar or $\hat{k}'$ axis is co-linear with the position vector $\vec{r}_c$ directed from the centroid of all fueled regions to the point at which the flux tally occurs. The fuelcentroid must be used because KENO V.a geometry can be input relative to any reference point. By using the centroid of the fueled region as a reference point, the consistency of the moment calculation is assured with differing models of the same system. The position and direction of travel of the particle, $\hat{\Omega}$, remain unchanged, but the spherical harmonics terms are calculated using this transformed coordinate system. This coordinate transform is illustrated inFigure 1. Here, $\hat{i}$, $\hat{j}$, and $\hat{k}$ represent the directional coordinate system axes, $m$, $h$, and $x$ represent the direction cosines, and $q$ and $r$ represent the polar and azimuthal angles of the "normal" coordinate system. The same symbols "primed" represent the transformed coordinate system. With the direction cosines consistently transformed for each history, the new polar and azimuthal angles can be computed and the spherical harmonics functions can be calculated for each history. The flux moments can then be tallied as shown inEq. (5).

## 2.2. SENSITIVITY COEFFICIENT GENERATION

Using the above methodologies to calculate the flux moments, all of the information necessary to generate sensitivity parameters using Monte Carlo methods is available. Methods used to generate the sensitivity coefficients are presented in this section. In operator notation, the neutron transport equation can be expressed as

$$A f = \frac{1}{k} B f \tag{6}$$

where

- $f$ = neutron flux;
- $k$ = eigenvalues and $k_{eff}$ is the largest of eigenvalues;
- $A$ = operator that represents all of the transport equation except for the fission term;
- $B$ = operator that represents the fission term of the transport equation.

The adjoint form of the transport equation can be expressed as

$$A^{\dagger} f^{\dagger} = \frac{1}{k} B^{\dagger} f^{\dagger}. \tag{7}$$

In the adjoint equation, the adjoint flux, $f^{\dagger}$, has a special physical significance as the "importance" of the particles within the system.

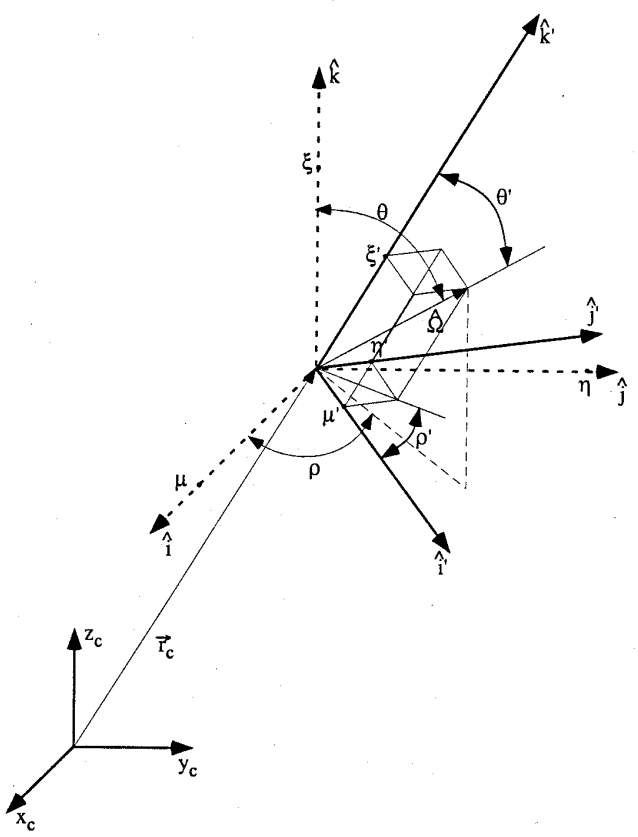


Figure 1. Coordinate System Transform for Spherical Harmonics Expansion.

Using linear perturbation theory, one may show that the relative change in $k$ due to a small perturbation in a macroscopic cross section, $\Sigma$, of the transport operator at some point in phase space $\vec{r}$ can be expressed as

$$S = \frac{dk/k}{d\Sigma(\vec{r})/\Sigma(\vec{r})} = -\frac{\Sigma(\vec{r})}{k}\frac{\left\langle f^{\dagger}(\vec{x})\left(\frac{dA[\Sigma(\vec{x})]}{d\Sigma(\vec{r})} - \frac{1}{k}\frac{dB[\Sigma(\vec{x})]}{d\Sigma(\vec{r})}\right)f(\vec{x})\right\rangle}{\left\langle f^{\dagger}(\vec{x})\frac{1}{k^2}B[\Sigma(\vec{x})]f(\vec{x})\right\rangle} \quad , \tag{8}$$

where $\vec{x}$ = phase space vector.

The $k$ sensitivity for individual cross sections can be obtained from Eq. (8) using the discrete-ordinates form of the transport equation. In doing so, the phase space vector, $\vec{x}$, has been replaced by indices representing discretization in space, energy and angle. The sensitivity coefficients are calculated in Eq. (9) for a given reaction $X$, isotope $i$, energy group, $g$, and computational region, $z$. Energy-integrated coefficients are obtained by summing the group-wise

coefficients over all energy groups. It has been demonstrated that the sensitivity coefficients can be represented as

$$S^i_{X,g,z} = \frac{1}{D}\left[T^i_{1,X,g,z} + T^i_{2,g,z} + T^i_{3,X,g,z}\right]. \tag{9}$$

where the denominator, *D*, is expressed as

$$D = \frac{1}{k}\sum_{i=1}^{I}\sum_{z=1}^{R} V_z \sum_{g=1}^{G}\left(n^i_{g,z}\Sigma^i_{f,g,z}\,f_{g,z}\right)\sum_{g'=1}^{G}\left(c^i_{g',z}\,f^*_{g',z}\right) \tag{10}$$

where

$c^i_{g',z}$ = average number of fission neutrons emitted into energy group $g'$ from fission of isotope *i* in region *z*;
$n^i_{g,z}$ = average number of fission neutrons emitted from fission of isotope *i* in region *z* in energy group *g*;
$\Sigma^i_{f,g,z}$ = macroscopic cross section for fission of isotope *i* in region *z* and energy group *g*;
*I* = number of isotopes;
*R* = number of computational regions;
*G* = number of neutron energy groups.

The first of the *T* terms can be expressed as

$$T^i_{1,X,g,z} = -\Sigma^i_{X,g,z} V_z \sum_{j=0}^{NMOM}(2\ell+1)\tilde{f}^{\dagger j}_{g,z}\tilde{f}^{\,j}_{g,z}\,, \tag{11}$$

where

$\Sigma^i_{X,g,z}$ = macroscopic cross section for some reaction X, of isotope i, energy group g, in region z;
$\ell$ = Legendre order that corresponds to the $j^{th}$ flux moment.

The second and third terms can be expressed as

$$T^i_{2,g,z} = \frac{1}{k} V_z n^i_{g,z}\Sigma^i_{f,g,z} f_{g,z}\sum_{g'=1}^{G} f^{\dagger}_{g',z} c_{g',z}\,; \tag{12}$$

$$T^i_{3,X,g,z} = \sum_{j=0}^{NMOM} V_z \sum_{g'=1}^{G}\tilde{f}^{\dagger j}_{g',z}\tilde{f}^{\,j}_{g,z}\Sigma^{\ell,i}_{X,g\to g',z} \tag{13}$$

where $\Sigma^{\ell,i}_{X,g\to g',z}$ = $\ell^{th}$ moment of the transfer cross section for reaction *X* of isotope *i*, from energy group *g* to energy group $g'$ in region *z*.

For specific reactions, not all of the $T$ terms defined above are needed to calculate the sensitivity coefficient. The application ofEq. (9) for each type of reaction is outlined below.

1. Absorption-Reaction Sensitivity (nonfission, nonscattering)

   Only the $T^i_{1,X,g,z}$ term is used for this class of reactions, where $\Sigma^i_{X,g,z}$ is the absorption cross section of interest ((n, $\gamma$), (n, $\alpha$), (n, p), etc.).

2. Fission-Reaction Sensitivity

   The fission reaction requires $T^i_{1,X,g,z}$ and $T^i_{2,g,z}$, where $\Sigma^i_{X,g,z}$ is the fission cross section.

3. $\bar{n}$ Sensitivity

   The $\bar{n}$ reaction only requires $T^i_{2,g,z}$.

4. $\chi$ Sensitivity

   The $\chi$ reaction only requires $T^i_{2,g,z}$, with the $c$ and $nS_f$ terms interchanged.

5. Scattering-Reaction Sensitivity

   All scattering reactions (elastic, inelastic, and (n, 2n) reactions) require $T^i_{1,X,g,z}$ and

   $T^i_{3,X,g,z}$, where $\Sigma^i_{X,g,z}$ is the scattering cross section and $\Sigma^{\ell,i}_{X,g\to g',k}$ is the group-to-group scattering matrix for the $\ell^{th}$ scattering moment.

6. Total-Reaction Sensitivity

   The total reaction requires $T^i_{1,X,g,z}$, $T^i_{2,g,z}$, and $T^i_{3,X,g,z}$. Here, $\Sigma^i_{X,g,z}$ is the total cross section and $\Sigma^{\ell,i}_{X,g\to g',k}$ is the group-to-group scattering matrix for the $\ell^{th}$ scattering moment. For nonfissionable isotopes, $T^i_{2,g,z}$ will be zero.

## 3. APPLICATION

The application of the perturbation methods and flux moment calculations outlined above for use in conjunction with the CSAS25 SCALE sequence was performed in two stages. The first step was to implement the flux moment computational methodology in the KENOV.a Monte Carlo code and to add the appropriate input parameters to the CSAS25 control sequence. The second stage included the design of the SAMS SCALE module that reads the restart data from the

forward and adjoint KENO V.a cases and calculates the sensitivity parameters for a given problem.

## 3.1. FLUX MOMENT CALCULATIONS

The calculation of the flux moments first required the calculation of the fuel centroid in KENO V.a. Next, a new subroutine was written to perform the coordinate transform and calculate the spherical harmonics functions for each history. Calls to this subroutine were added to each point where the flux tallies occur. The average spherical harmonics functions for a particular track are calculated from those sampled at five points along each track. This step is necessary because the angle between the direction of travel and the position vector (measured relative to the centroid of the fueled region) can change significantly over the length of a given track. For adjoint problems, the spherical harmonics functions are determined for the reflected angle from the direction of travel. An input parameter was added to the CSAS25 sequence to allow the selection of the order through which the flux moments are calculated. This parameter does not affect the scattering order used by KENO V.a in the calculation of collisions. With the calculation of the flux moments, the run time for KENO V.a is increased by approximately a factor of 4 for first-order moments and a factor of 8 for third-order moments.

## 3.2. DESIGN OF THE SAMS MODULE

The SAMS module was designed to run under the SCALE driver in conjunction with the other modules of the SCALE code system. It reads binary files that are produced from forward and adjoint CSAS25 analyses of the same system with exactly the same geometry input and cross-section libraries. The number of particle histories or generations is only used for statistical uncertainty analyses, and different numbers of histories are permitted in the forward and adjoint cases. A flow diagram showing the execution of SAMS and the required CSAS25 cases under the SCALE driver is indicated in Figure 2. The interface files are shown in this diagram as ovals, and the default filenames are also shown. Note that every sequence that is executed displays its printed output in a single SCALE output file.

SAMS reads the binary data files written by the CSAS25 module for the forward and adjoint cases of the system model. It automatically checks for available data for each nuclide on the cross-section data file and prepares a list of sensitivity parameters that can be calculated for each nuclide. It then calculates the sensitivity parameters for each nuclide for each region that contains that nuclide on a group-wise basis. Once all of the group-wise sensitivity parameters have been calculated, they are summed to produce energy- and region-integrated values.

SAMS offers several choices for data output. The standard text output file always includes the sensitivity values and their associated uncertainties integrated over energy and region for every nuclide and reaction. At the discretion of the user, the output may also include the total cross-section sensitivity parameters for each nuclide summed over the material index used in KENO V.a. The user may also select an option to view sensitivity parameters for every region in the problem description. If this option is chosen, data describing the region are read from the KENO V.a restart file and are presented for the convenience of the user. After the region description, all of the energy-integrated sensitivity parameters that were calculated for each nuclide in that region are presented.

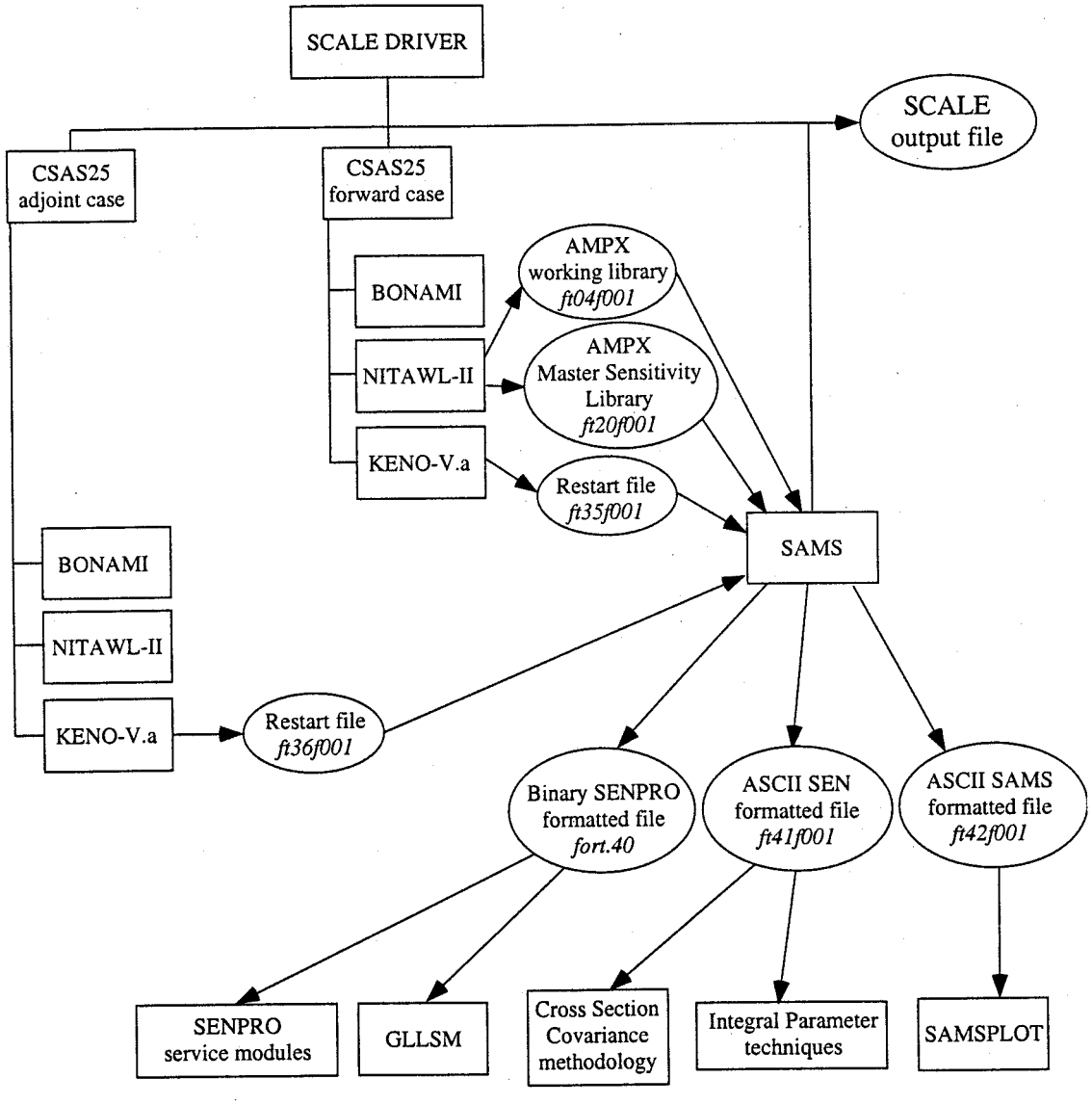


Figure 2. Flow Diagram of SAMS and CSAS25 with the SCALE Driver.

SAMS also presents group-wise sensitivity data in three sensitivity file formats. The first is the SENPRO format that was introduced with the FORSS system. SAMS also presents similar data in the SEN format that are compatible with the SEN1/SEN2 sequences. The integral parameter techniques, cross-section covariance methodology and GLLSM packages used for range of applicability work read the sensitivity profiles in this format. The SENPLT two-dimensional plotting program also reads data in this format. The new SAMS formatted sensitivity file is

similar to the SEN format, but it also allows for the sensitivity parameter uncertainties to be stored along with the sensitivity values. This format also allows for the recording of data describing each region, a feature that is not currently available in the other file formats. This file format is read by the SAMSPLOT program to produce 2-D sensitivity plots including error bars to display the statistical uncertainties due to Monte Carlo techniques.

# 4. RESULTS

The sensitivity results generated with SAMS have been verified by two methods. First, a simple test case was analyzed using both SEN1 and SAMS, and the results were compared. Second, a more complex test case was analyzed with both SEN2 and SAMS, and the results were compared. Since the deterministic codes do not directly output the flux moments, a direct comparison with the KENO V.a calculated moments would be difficult. However, because the sensitivity results are calculated from the flux moments, validation of the sensitivities can be used to validate the calculation of the moments for this application. For all of the cases presented in this chapter, the KENO V.a flux moments were calculated to the third order. Also, all calculations were performed using the 44-group ENDF/B-V SCALE library.

## 4.1. COMPARISONS WITH SEN1

To verify that the results generated with SAMS were consistent with those generated with SEN1, a critical experiment that could be easily modeled in SEN1 and KENOV.a was analyzed. The selected sample problem is based on an unreflected rectangular parallelpiped containing a homogeneous mixture $UF_4$ and paraffin with an enrichment of 2% in $^{235}U$. The $H/^{235}U$ atomic ratio is 293.9:1. The dimensions of the experiment were 56.22 cm $\times$ 56.22 cm $\times$ 122.47 cm.[15] This critical experiment is designated as CAS14. For consistency, in both SEN1 and SAMS, this experiment was modeled as a sphere of the mixture material with a critical radius of 38.50 cm.

When this experiment was modeled as a single region using CSAS25 with SAMS-generated sensitivities, the nonscattering reaction sensitivity parameters compared favorably with the SEN1 results, but the SAMS sensitivities-to-scattering reactions, including the total sensitivity, were not as consistent. The sphere was then divided into nine spherical shells, and the sensitivities were recalculated. The sensitivity parameter results for all of the reaction types for all of the nuclides then compared much more favorably. These results are shown in Table I. The differences in the results from the two KENOV.a models are due to the summation of the product of the forward and adjoint fluxes over the regions in the problem. For a region in which the flux moments vary greatly by position, sub-dividing will produce more accurate results. However, in this approach, note that increasing the number of computational regions increases the run time for the problem. For these cases, the forward analyses in KENOV.a were executed with 1000 histories per generation and 1000 generations. For the adjoint cases, the numbers of histories per generation were increased to 2000.

Table I. Energy-Integrated Sensitivities for Spherical Models of CAS14

| Isotope | Reaction | SEN1 $k_{eff}$ = 1.0045 | SAMS (single region) $k_{eff}$ = 1.0037 ± 0.0008 | SAMS (nine regions) $k_{eff}$ = 1.0037 ± 0.0008 |
|---|---|---|---|---|
| $^{1}$H | Total | 2.89E-01 | 3.10E-01 ± 1.56E-02 | 2.87E-01 ± 1.75E-02 |
| $^{1}$H | Scatter | 3.91E-01 | 4.10E-01 ± 1.55E-02 | 3.88E-01 ± 1.74E-02 |
| $^{1}$H | Elastic | 3.91E-01 | 4.10E-01 ± 1.55E-02 | 3.88E-01 ± 1.74E-02 |
| $^{1}$H | Capture | -1.01E-01 | -1.00E-01 ± 3.48E-05 | -1.01E-01 ± 1.67E-05 |
| $^{1}$H | n,γ | -1.01E-01 | -1.00E-01 ± 3.48E-05 | -1.01E-01 ± 1.67E-05 |
| $^{12}$C | Total | 3.20E-02 | 4.16E-02 ± 9.15E-04 | 3.19E-02 ± 9.95E-04 |
| $^{12}$C | Scatter | 3.27E-02 | 4.23E-02 ± 9.14E-04 | 3.26E-02 ± 9.94E-04 |
| $^{12}$C | Elastic | 3.24E-02 | 4.20E-02 ± 9.14E-04 | 3.23E-02 ± 9.94E-04 |
| $^{12}$C | n,n' | 2.48E-04 | 2.62E-04 ± 1.29E-05 | 2.57E-04 ± 1.07E-05 |
| $^{12}$C | Capture | -6.70E-04 | -6.73E-04 ± 1.02E-06 | -6.67E-04 ± 4.04E-07 |
| $^{12}$C | n, γ | -4.98E-04 | -4.92E-04 ± 1.70E-07 | -4.96E-04 ± 8.14E-08 |
| $^{12}$C | n,p | -3.10E-08 | -3.30E-08 ± 2.76E-10 | -3.11E-08 ± 1.07E-10 |
| $^{12}$C | n,d | -7.84E-08 | -8.33E-08 ± 6.97E-10 | -7.86E-08 ± 2.71E-10 |
| $^{12}$C | n,α | -1.72E-04 | -1.80E-04 ± 1.01E-06 | -1.71E-04 ± 3.95E-07 |
| $^{19}$F | Total | 4.79E-02 | 6.29E-02 ± 1.28E-03 | 4.78E-02 ± 1.30E-03 |
| $^{19}$F | Scatter | 5.34E-02 | 6.85E-02 ± 1.27E-03 | 5.33E-02 ± 1.30E-03 |
| $^{19}$F | Elastic | 3.75E-02 | 4.96E-02 ± 9.17E-04 | 3.75E-02 ± 9.93E-04 |
| $^{19}$F | n,n' | 1.59E-02 | 1.88E-02 ± 5.34E-04 | 1.58E-02 ± 5.03E-04 |
| $^{19}$F | n,2n | 3.28E-06 | 2.23E-05 ± 2.02E-07 | 2.11E-05 ± 1.70E-07 |
| $^{19}$F | Capture | -5.51E-03 | -5.55E-03 ± 6.06E-06 | -5.52E-03 ± 2.58E-06 |
| $^{19}$F | n, γ | -2.33E-03 | -2.31E-03 ± 7.51E-07 | -2.32E-03 ± 3.61E-07 |
| $^{19}$F | n,p | -2.17E-04 | -2.24E-04 ± 6.84E-07 | -2.17E-04 ± 2.80E-07 |
| $^{19}$F | n,d | -1.06E-05 | -1.12E-05 ± 7.14E-08 | -1.06E-05 ± 2.79E-08 |
| $^{19}$F | n,t | -2.33E-06 | -2.48E-06 ± 2.07E-08 | -2.34E-06 ± 8.04E-09 |
| $^{19}$F | n,α | -2.95E-03 | -3.00E-03 ± 5.51E-06 | -2.97E-03 ± 2.35E-06 |
| $^{235}$U | Total | 2.53E-01 | 2.60E-01 ± 9.92E-04 | 2.56E-01 ± 1.08E-03 |
| $^{235}$U | Scatter | 4.52E-04 | 5.87E-04 ± 6.05E-06 | 4.51E-04 ± 6.28E-06 |
| $^{235}$U | Elastic | 2.87E-04 | 4.02E-04 ± 4.27E-06 | 2.87E-04 ± 4.92E-06 |
| $^{235}$U | n,n' | 1.57E-04 | 1.76E-04 ± 4.10E-06 | 1.56E-04 ± 3.73E-06 |
| $^{235}$U | n,2n | 1.10E-05 | 3.08E-05 ± 1.95E-07 | 2.99E-05 ± 1.65E-07 |
| $^{235}$U | Fission | 3.65E-01 | 3.70E-01 ± 8.94E-04 | 3.67E-01 ± 9.55E-04 |
| $^{235}$U | Capture | -1.12E-01 | -1.11E-01 ± 3.52E-05 | -1.12E-01 ± 1.69E-05 |
| $^{235}$U | n, γ | -1.12E-01 | -1.11E-01 ± 3.52E-05 | -1.12E-01 ± 1.69E-05 |
| $^{235}$U | $\bar{n}$ | 9.50E-01 | 9.49E-01 ± 4.19E-04 | 9.50E-01 ± 1.95E-04 |
| $^{235}$U | χ | 9.50E-01 | 9.49E-01 ± 4.68E-04 | 9.50E-01 ± 2.17E-04 |
| $^{238}$U | Total | -2.87E-01 | -2.75E-01 ± 5.61E-04 | -2.86E-01 ± 5.84E-04 |
| $^{238}$U | Scatter | 2.78E-02 | 3.53E-02 ± 3.22E-04 | 2.77E-02 ± 3.11E-04 |
| $^{238}$U | Elastic | 1.42E-02 | 2.00E-02 ± 1.55E-04 | 1.42E-02 ± 1.79E-04 |
| $^{238}$U | n,n' | 1.25E-02 | 1.42E-02 ± 2.75E-04 | 1.25E-02 ± 2.48E-04 |
| $^{238}$U | n,2n | 1.01E-03 | 2.90E-03 ± 2.39E-05 | 2.78E-03 ± 2.02E-05 |
| $^{238}$U | Fission | 3.37E-02 | 3.46E-02 ± 5.43E-05 | 3.38E-02 ± 4.65E-05 |
| $^{238}$U | Capture | -3.49E-01 | -3.45E-01 ± 1.26E-04 | -3.47E-01 ± 6.54E-05 |
| $^{238}$U | n, γ | -3.49E-01 | -3.45E-01 ± 1.26E-04 | -3.47E-01 ± 6.54E-05 |
| $^{238}$U | $\bar{n}$ | 5.04E-02 | 5.14E-02 ± 2.91E-05 | 5.05E-02 ± 1.32E-05 |
| $^{238}$U | χ | 5.04E-02 | 5.14E-02 ± 2.54E-05 | 5.05E-02 ± 1.15E-05 |

Some differences in the calculated sensitivities from SEN1 and SAMS occur as a result of threshold reactions such as (n,2n). This discrepancy is likely due to inadequate sampling in the determination of adjoint flux at high energy for this thermal system. Although the scalar flux has probably been adequately sampled, the flux moments may not also have been calculated as accurately as necessary. However, threshold reactions make only a small contribution to the sensitivity of the system $k_{eff}$. For example, for $^{235}$U, the sensitivity to the (n,2n) reaction is four orders of magnitude smaller than the sensitivity to the total cross section.

It is evident that for nonscattering reactions, such as capture and $\bar{n}$, the calculated sensitivity values are accurately calculated with much less geometrical division than is needed for the scattering reactions. This indicates that the correct product of the forward and adjoint scalar fluxes is more easily obtained than the same product for the flux moments.

Region integrated energy dependent sensitivity profiles from SEN1 and SAMS for selected reactions are shown in Figures. 3 through 6. The SAMS data are presented for the nine-region spherical case. Figures 3 and 4 depict the scattering sensitivity for $^{1}$H. These profiles agree well, except at low energies, where the uncertainties in the SAMS data mask the characteristics observable in the SEN1 plot. However, note that these data are two orders of magnitude below the peak group-wise sensitivity and contribute very little to the energy-integrated value. These large uncertainties in the scattering profiles were traced to the method used to calculate the scattering sensitivities. For scattering sensitivities, the $T_1$ term shown in Eq. (11) that utilizes the 1-D scattering cross section is added to the $T_3$ term shown in Eq. (13) that utilizes the full 2-D scattering matrix. These terms have nearly equal magnitudes and opposite signs. Each term has an associated uncertainty that is propagated through their addition. Even though the sum of the terms produces a value much smaller than either of the original values, the magnitude of the uncertainty essentially remains unchanged. The statistical uncertainty in the sensitivities is slowly reduced as the number of histories in the KENO V.a calculation is increased.

Figures 5 and 6 show the sensitivity to the fission cross section of $^{235}$U. These plots display excellent agreement between SEN1 and SAMS over the entire energy range. The comparisons to SEN1 for the first test case demonstrate that SAMS correctly computes sensitivities for all reaction types if the KENO V.a model is divided in a manner that allows for the products of the forward and adjoint fluxes to be computed accurately.

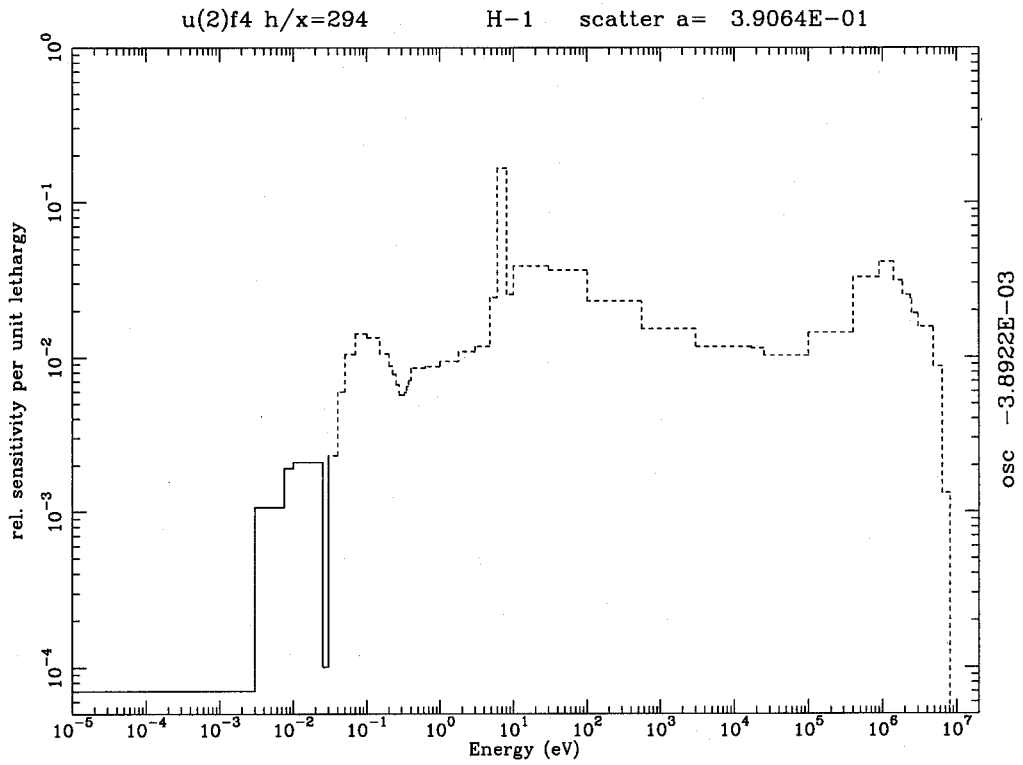


Figure 3. SEN1-Generated $^{1}$H Sensitivity-to-Scattering Cross Section for CAS14.

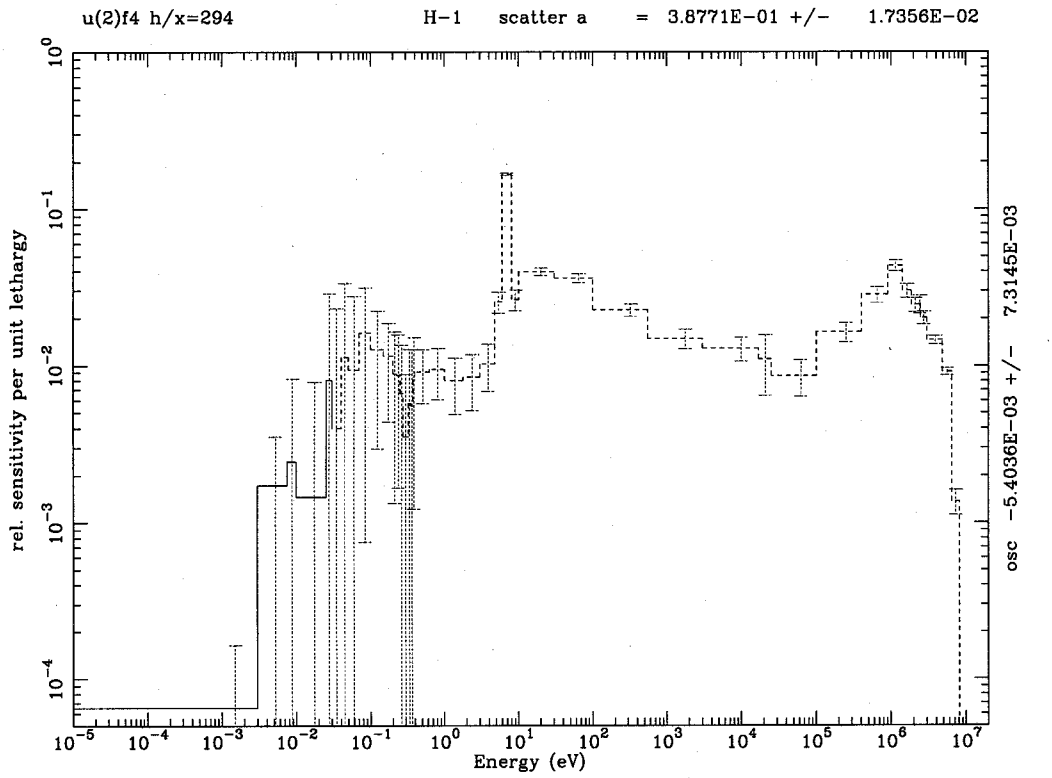


Figure 4. SAMS-Generated $^{1}$H Sensitivity-to-Scattering Cross Section for CAS14.

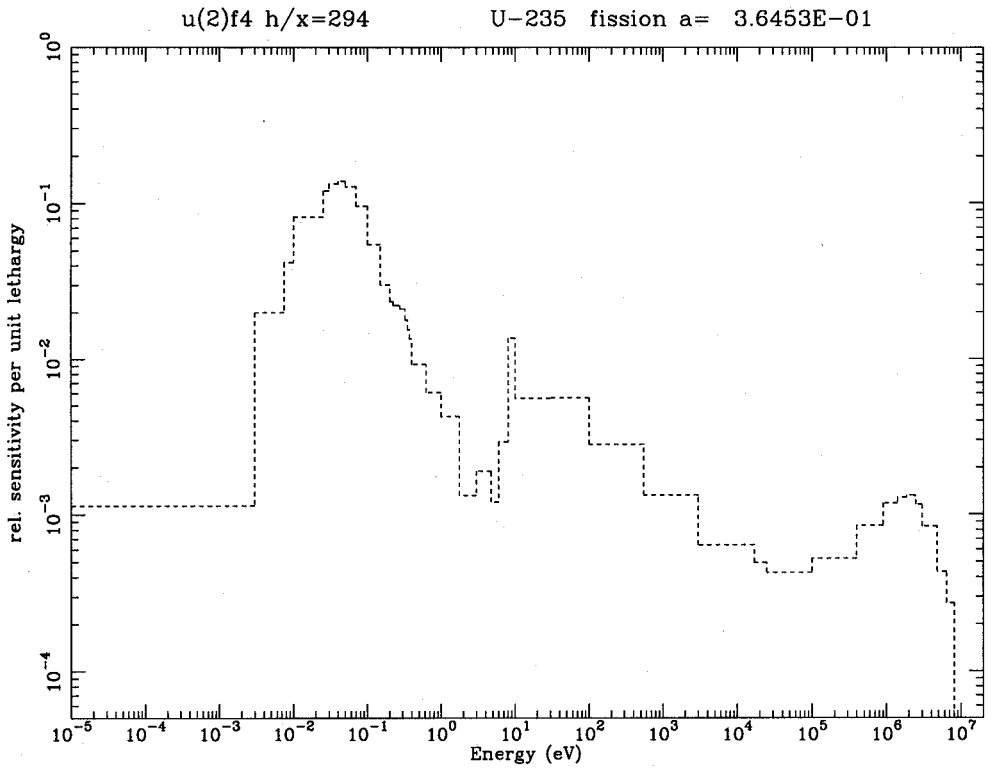


Figure 5. SEN1-Generated $^{235}$U Sensitivity-to-FissionCross Section for CAS14.

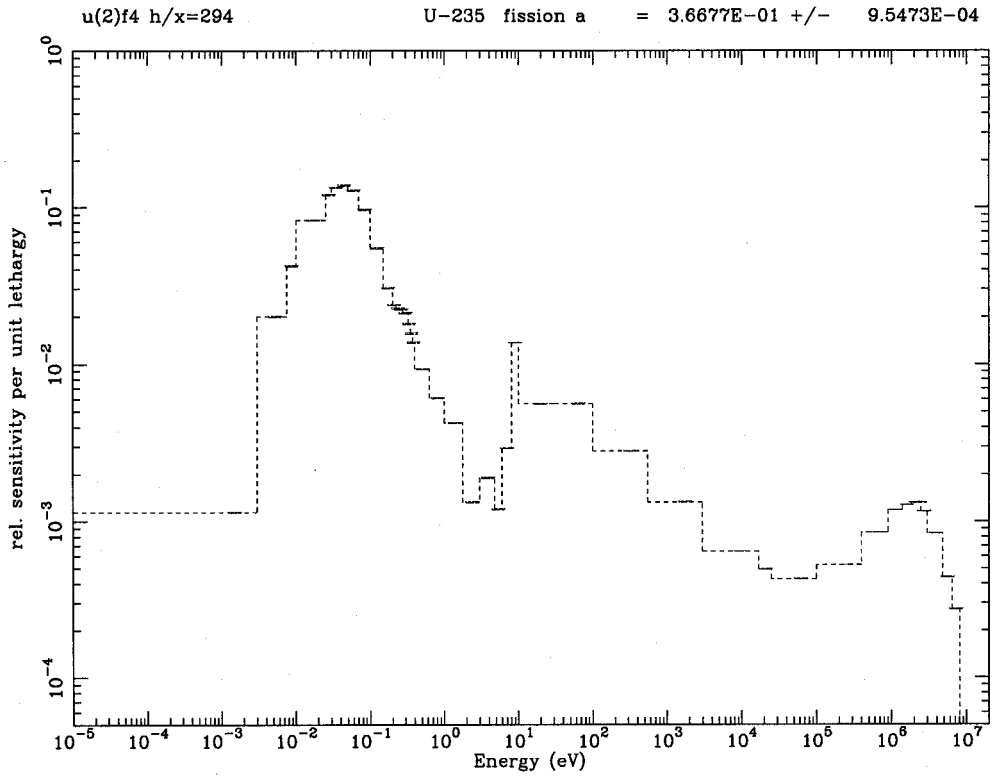


Figure 6. SAMS-Generated $^{235}$U Sensitivity-to-FissionCross Section for CAS14.

## 4.2. COMPARISON WITH SEN2

To verify the accuracy of the SAMS calculations for more complex geometrical configurations, the SHEBA-II[16,17] experiment was calculated. The critical assembly vessel (CAV) consists of a cylindrical tank which is essentially a 73.7-cm length of 50.8-cm OD stainless steel pipe. A safety rod thimble with a 6 cm OD passes through the center of the CAV. The tank is filled to a critical height of 43.5 cm with a 5% enriched solution of $UO_2F_2$ and water. The SAMS-generated sensitivities were compared with the SEN2 sensitivities for three different KENO V.a models. In the first KENO V.a model, the fuel was contained within a single region. Then, in the second KENO V.a model, the fuel was divided axially and radially into four regions to determine if the sensitivity data changed with smaller geometrical regions. In the third KENO V.a model, the fuel was further divided into a total of 12 regions. Scoping calculations revealed that no significant changes in the sensitivity results were realized by further dividing the geometry. The energy and region integrated results from the different KENO V.a analyses, and the corresponding SEN2 results are shown in Table II. For both the forward and adjoint analyses, the KENO V.a cases were performed with 2000 histories per generation and 1000 generations.

It can be seen in Table II that the SAMS results, even for a single fuel region, agree reasonably well with the SEN2 results for most reactions and nuclides. The results converge quickly as the number of regions is increased. As with the previous test case, the largest discrepancies occur for threshold reactions.

The sensitivity profiles for the Fe-scattering cross section for all of the stainless steel in the model are presented in Figures 7 and 8 for SEN2 and SAMS, respectively. These results are quite similar and validate the use of SAMS for calculating sensitivities in nonfueled regions. For the fueled regions, the sensitivity profiles (not shown) demonstrate characteristics similar to those for the previous test case and display excellent agreement between the two codes.

Table II. Energy Integrated Sensitivities for SHEBA-II Verification Case

| Isotope | Reaction | SEN2 $k_{eff}$ = 1.0028 | SAMS (single fuel region) $k_{eff}$ = 1.0034 ± 0.0007 | SAMS (four fuel regions) $k_{eff}$ = 1.0037 ± 0.0006 | SAMS (12 fuel regions) $k_{eff}$ = 1.0038 ± 0.0006 |
|---|---|---|---|---|---|
| $^{1}$H | Total | 3.35E-01 | 3.38E-01 ± 2.23E-02 | 3.35E-01 ± 2.54E-02 | 3.33E-01 ± 2.55E-02 |
| $^{1}$H | Scatter | 4.83E-01 | 4.83E-01 ± 2.22E-02 | 4.81E-01 ± 2.52E-02 | 4.81E-01 ± 2.53E-02 |
| $^{1}$H | Elastic | 4.83E-01 | 4.83E-01 ± 2.22E-02 | 4.81E-01 ± 2.52E-02 | 4.81E-01 ± 2.53E-02 |
| $^{1}$H | Capture | -1.48E-01 | -1.45E-01 ± 4.29E-05 | -1.46E-01 ± 1.99E-05 | -1.48E-01 ± 2.09E-05 |
| $^{1}$H | n,γ | -1.48E-01 | -1.45E-01 ± 4.29E-05 | -1.46E-01 ± 1.99E-05 | -1.48E-01 ± 2.09E-05 |
| $^{16}$O | Total | 7.18E-02 | 8.10E-02 ± 1.31E-03 | 7.68E-02 ± 1.43E-03 | 7.24E-02 ± 1.43E-03 |
| $^{16}$O | Scatter | 7.40E-02 | 8.32E-02 ± 1.31E-03 | 7.90E-02 ± 1.43E-03 | 7.46E-02 ± 1.43E-03 |
| $^{16}$O | Elastic | 7.35E-02 | 8.27E-02 ± 1.31E-03 | 7.85E-02 ± 1.43E-03 | 7.41E-02 ± 1.43E-03 |
| $^{16}$O | n,n' | 4.80E-04 | 4.75E-04 ± 7.87E-06 | 4.73E-04 ± 6.64E-06 | 4.70E-04 ± 6.50E-06 |
| $^{16}$O | Capture | -2.19E-03 | -2.25E-03 ± 3.15E-06 | -2.24E-03 ± 2.50E-06 | -2.21E-03 ± 1.92E-06 |
| $^{16}$O | n, γ | -5.10E-05 | -4.98E-05 ± 1.47E-08 | -5.01E-05 ± 6.82E-09 | -5.09E-05 ± 7.16E-09 |
| $^{16}$O | n,p | -4.73E-06 | -4.86E-06 ± 3.13E-08 | -4.79E-06 ± 2.73E-08 | -4.78E-06 ± 2.04E-08 |
| $^{16}$O | n,d | -9.69E-07 | -9.97E-07 ± 6.42E-09 | -9.82E-07 ± 5.59E-09 | -9.80E-07 ± 4.19E-09 |
| $^{16}$O | n,α | -2.13E-03 | -2.19E-03 ± 3.13E-06 | -2.18E-03 ± 2.49E-06 | -2.15E-03 ± 1.91E-06 |
| Fe | Total | 1.66E-02 | 1.79E-02 ± 1.79E-04 | 1.69E-02 ± 1.56E-04 | 1.56E-02 ± 1.46E-04 |
| Fe | Scatter | 2.28E-02 | 2.49E-02 ± 1.45E-04 | 2.32E-02 ± 1.27E-04 | 2.15E-02 ± 1.19E-04 |
| Fe | Elastic | 1.96E-02 | 2.12E-02 ± 1.33E-04 | 1.98E-02 ± 1.16E-04 | 1.84E-02 ± 1.08E-04 |
| Fe | n,n' | 3.22E-03 | 3.64E-03 ± 5.03E-05 | 3.39E-03 ± 4.49E-05 | 3.13E-03 ± 4.20E-05 |
| Fe | n,2n | 2.91E-05 | 1.03E-05 ± 1.65E-07 | 9.62E-06 ± 1.53E-07 | 8.32E-06 ± 1.31E-07 |
| Fe | Capture | -6.22E-03 | -6.92E-03 ± 7.63E-06 | -6.28E-03 ± 7.23E-06 | -5.93E-03 ± 6.54E-06 |
| Fe | n, γ | -6.18E-03 | -6.88E-03 ± 7.62E-06 | -6.25E-03 ± 7.22E-06 | -5.89E-03 ± 6.53E-06 |
| Fe | n,p | -3.22E-05 | -3.69E-05 ± 2.65E-07 | -3.44E-05 ± 2.50E-07 | -3.13E-05 ± 2.23E-07 |
| Fe | n,d | -1.17E-07 | -1.06E-08 ± 4.75E-10 | -1.03E-08 ± 4.60E-10 | -8.26E-09 ± 4.02E-10 |
| Fe | n,t | -4.32E-09 | -3.35E-11 ± 1.51E-12 | -3.25E-11 ± 1.46E-12 | -2.61E-11 ± 1.27E-12 |
| Fe | n,α | -1.64E-06 | -1.74E-06 ± 3.32E-08 | -1.65E-06 ± 3.20E-08 | -1.44E-06 ± 2.80E-08 |
| $^{235}$U | Total | 2.45E-01 | 2.61E-01 ± 1.14E-03 | 2.57E-01 ± 1.25E-03 | 2.47E-01 ± 1.26E-03 |
| $^{235}$U | Scatter | 6.90E-04 | 7.57E-04 ± 5.84E-06 | 7.23E-04 ± 6.36E-06 | 6.92E-04 ± 6.36E-06 |
| $^{235}$U | Elastic | 3.85E-04 | 4.43E-04 ± 4.85E-06 | 4.14E-04 ± 5.61E-06 | 3.84E-04 ± 5.66E-06 |
| $^{235}$U | n,n' | 2.95E-04 | 3.03E-04 ± 3.13E-06 | 2.98E-04 ± 2.86E-06 | 2.96E-04 ± 2.77E-06 |
| $^{235}$U | n,2n | 1.41E-05 | 3.36E-05 ± 1.35E-07 | 3.34E-05 ± 1.17E-07 | 3.32E-05 ± 1.16E-07 |
| $^{235}$U | Fission | 3.61E-01 | 3.74E-01 ± 1.02E-03 | 3.70E-01 ± 1.10E-03 | 3.62E-01 ± 1.11E-03 |
| $^{235}$U | Capture | -1.16E-01 | -1.13E-01 ± 3.12E-05 | -1.14E-01 ± 1.45E-05 | -1.16E-01 ± 1.52E-05 |
| $^{235}$U | n, γ | -1.16E-01 | -1.13E-01 ± 3.12E-05 | -1.14E-01 ± 1.45E-05 | -1.16E-01 ± 1.52E-05 |
| $^{235}$U | $\bar{n}$ | 9.83E-01 | 9.82E-01 ± 3.61E-04 | 9.82E-01 ± 1.60E-04 | 9.82E-01 ± 1.68E-04 |
| $^{235}$U | χ | 9.83E-01 | 9.82E-01 ± 3.90E-04 | 9.82E-01 ± 1.73E-04 | 9.82E-01 ± 1.82E-04 |
| $^{238}$U | Total | -1.40E-01 | -1.37E-01 ± 2.73E-04 | -1.39E-01 ± 2.95E-04 | -1.40E-01 ± 2.93E-04 |
| $^{238}$U | Scatter | 1.77E-02 | 1.92E-02 ± 1.10E-04 | 1.85E-02 ± 1.11E-04 | 1.78E-02 ± 1.10E-04 |
| $^{238}$U | Elastic | 7.94E-03 | 9.17E-03 ± 6.89E-05 | 8.57E-03 ± 7.97E-05 | 7.94E-03 ± 8.04E-05 |
| $^{238}$U | n,n' | 9.27E-03 | 9.55E-03 ± 8.35E-05 | 9.39E-03 ± 7.53E-05 | 9.32E-03 ± 7.31E-05 |
| $^{238}$U | n,2n | 5.16E-04 | 1.23E-03 ± 6.36E-06 | 1.22E-03 ± 5.52E-06 | 1.21E-03 ± 5.51E-06 |
| $^{238}$U | Fission | 1.23E-02 | 1.26E-02 ± 1.68E-05 | 1.25E-02 ± 1.46E-05 | 1.24E-02 ± 1.42E-05 |
| $^{238}$U | Capture | -1.70E-01 | -1.69E-01 ± 5.53E-05 | -1.70E-01 ± 3.20E-05 | -1.70E-01 ± 3.04E-05 |
| $^{238}$U | n, γ | -1.70E-01 | -1.69E-01 ± 5.53E-05 | -1.70E-01 ± 3.20E-05 | -1.70E-01 ± 3.04E-05 |
| $^{238}$U | $\bar{n}$ | 1.75E-02 | 1.77E-02 ± 7.96E-06 | 1.77E-02 ± 3.51E-06 | 1.75E-02 ± 3.61E-06 |
| $^{238}$U | χ | 1.75E-02 | 1.77E-02 ± 7.06E-06 | 1.77E-02 ± 3.11E-06 | 1.75E-02 ± 3.21E-06 |

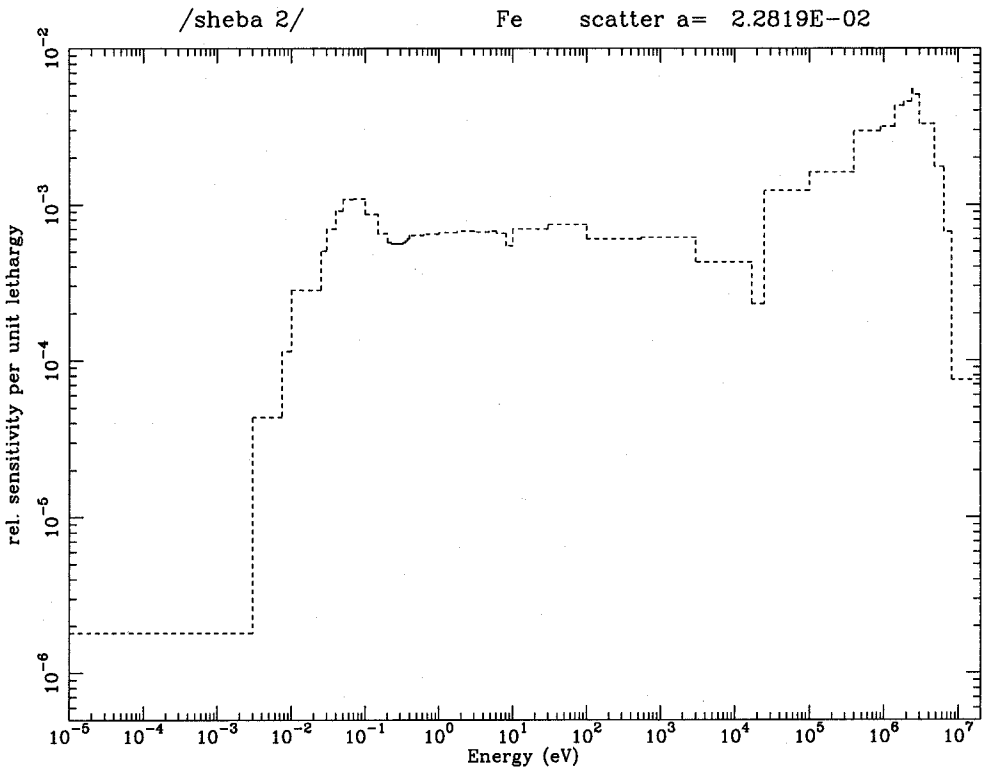


Figure 7. SEN2-Generated Fe Sensitivity-to-Scattering Cross Section for SHEBA-II.

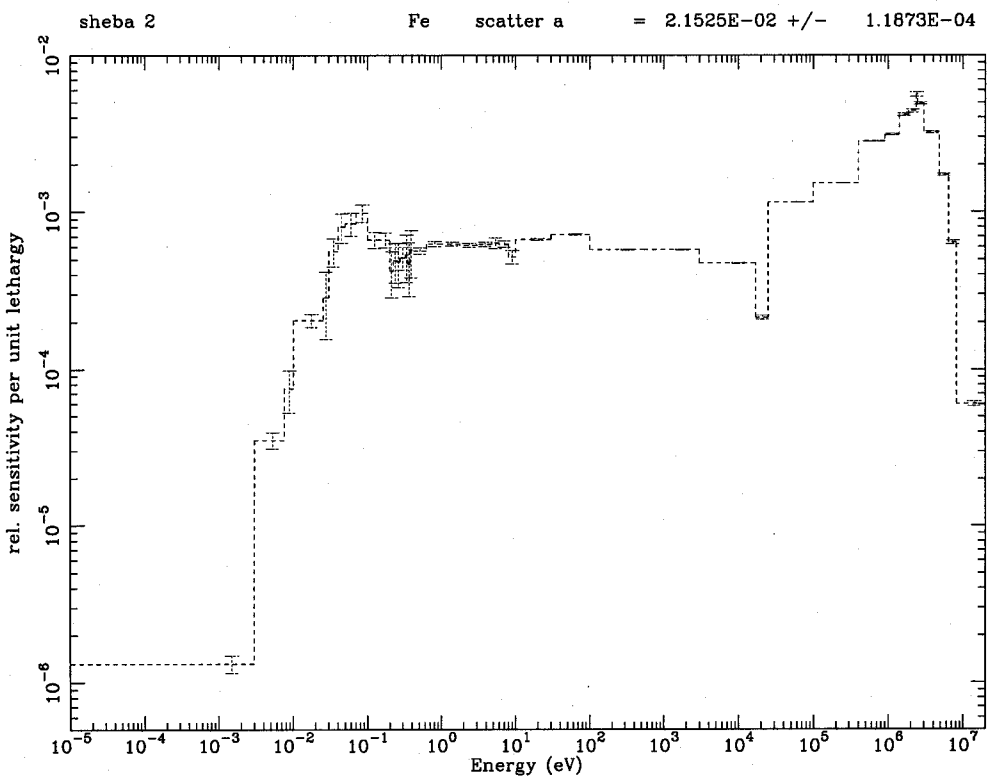


Figure 8. SAMS-Generated Fe Sensitivity-to-Scattering Cross Section for SHEBA-II.

# 5. CONCLUSIONS

With the SAMS module, the sensitivity of $k_{eff}$ to a large number of nuclear data parameters for nuclear criticality models can be assessed using first-order multigroup perturbation theory within the CSAS25 SCALE sequence. With proper specification of the problem geometry, SAMS has been demonstrated to show good agreement with the 1-D and 2-D PTCs SEN1 and SEN2. The sensitivities for any nuclide-reaction pair calculated with SAMS can be output on three bases: group-wise region dependent, energy-integrated region dependent, and energy and region integrated. These bases give the user the ability to interpret the data with varying levels of detail. SAMS produces sensitivities in a number of convenient formats for further analysis, either manually or with other automated techniques. SAMS produces the data necessary for evaluations with the integral parameter applications and cross-section covariance theory, as well as GLLSM. Using sensitivity parameters generated from 3-D models with SAMS, the number of critical experiments and applications that can be analyzed with the S/U techniques has been greatly increased.

## REFERENCES


1. B. L. Broadhead, C. M. Hopper, R. L. Childs, and C. V. Parks, *Sensitivity and Uncertainty Analyses Applied to Criticality Validation, Volume 1: Methods Development*, NUREG/CR-5593, Vol. 1 (ORNL/TM-13692/V1), U.S. Nuclear Regulatory Commission, Oak Ridge National Laboratory (1999).

2. *SCALE: A Modular Code System for Performing Standardized Computer Analyses for Licensing and Evaluations*, NUREG/CR-0200, Rev. 5 (ORNL/NUREG/CSD-2R5), Vols. I, II, and III, (March 1997). Available from Radiation Safety Information Computational Center at Oak Ridge National Laboratory as CCC-545.

3. J. L. Lucius et al., *A Users Manual for the FORSS Sensitivity and Uncertainty Analysis Code System*, ORNL-5316, Union Carbide Corp., Oak Ridge National Laboratory (1981).

4. C. R. Weisbin, E. M. Oblow, J. H. Harable, R. W. Peele, and J. L. Lucius, "Application of Sensitivity and Uncertainty Methodology to Fast Reactor Integral Experiment Analysis," *Nucl. Sci. Eng.*, **66**, 307 (1978).

5. C. R. Weisbin et al., *Application of FORSS Sensitivity and Uncertainty Methodology to Fast Reactor Benchmark Analysis*, ORNL/TM-5563, Union Carbide Corp., Oak Ridge National Laboratory (1976).

6. E. M. Oblow, "Sensitivity Theory from a Differential Viewpoint," *Nucl. Sci. Eng.*, **59**, 187 (1976).

7. W. M. Stacey, Jr., "Variational Estimates of Reactivity Worths and Reaction Rate Ratios in Critical Nuclear Reactors," *Nucl. Sci. Eng.*, **48**, 444 (1972).

8. L. N. Usachev, "Perturbation Theory for the Breeding Ratio and for Other Number Ratios Pertaining to Various Reactor Processes," *J. Nucl. Energy*, Pts A/B, **18**, 571 (1964).

9. A. Gandini, "A Generalized Perturbation Method of the Real and Adjoint Neutron Fluxes," *J. Nucl. Energy*, **21**, 755 (1967).

10. R. L. Childs, *SEN1: A One Dimensional Cross-Section Sensitivity and Uncertainty Module for Criticality Safety Analysis*, NUREG/CR-5719 (ORNL/TM-13738), U.S. Nuclear Regulatory Commission, Oak Ridge National Laboratory (1999).

11. B. T. Rearden, *Development of SAMS: A Sensitivity Analysis Module for the SCALE Code System Using KENO V.a in the CSAS25 Sequence*, Ph.D. Dissertation, Texas A&M University (1999).

12. R. D. O'Dell and R. E. Alcouffe, *Transport Calculations for Nuclear Analyses: Theory and Guidelines for Effective Use of Transport Codes*, LA-10983-MS, Los Alamos National Laboratory (September 1987).

13. E. E. Lewis and W. F. Miller, Jr., *Computational Methods of Neutron Transport*, American Nuclear Society, La Grange Park, IL (1993).

14. L. L. Carter and E. D. Cashwell, "Particle-Transport Simulation with the Monte Carlo Method," TID-26607, U.S. Energy Research and Development Administration (1975).

15. W. C. Jordan, N. F. Landers, and L. M. Petrie, "Validation of KENO V.a Comparison with Critical Experiments," ORNL/CSD/TM-238, Martin Marietta Energy Systems, Oak Ridge National Laboratory (December 1986).

16. *International Handbook of Evaluated Criticality Safety Benchmark Experiments*, Nuclear Energy Agency Nuclear Science Committee of the Organization for Economic Co-operation and Development, NEA/NSC/DOC(95)03, Paris (1998).

17. K. B. Butterfield, "The SHEBA Experiment," *Trans. Am. Nucl. Soc.*, **70**, 199 (1994).